

# Interplay between topological interface states in four-terminal conductance of quantum Hall graphene

Nojoon Myoung and Hee Chul Park\*

*Center for Theoretical Physics of Complex Systems,  
Institute for Basic Science, Daejeon 34051, Republic of Korea*

(Dated: February 3, 2017)

## Abstract

We investigate the interplay behaviour of the topologically protected states at the interface of Chern insulator junctions generated by quantum Hall graphene systems. Four-terminal quantum Hall conductance is exploited to understand how the states are coupled to each other at the interface. We demonstrate that the interplay of the topological states occurs only between the time-reversal partners characterized by the same Chern number, using the Chalker-Coddington type argument. We also find interplay suppression, depending on how the Chern insulator junction is fabricated.

## INTRODUCTION

Graphene is a promising material for studying quantum Hall effects with gate-tunable filling factors on account of its capability for controlling charge density via field effects[1, 2]. Studies involving conductance measurements through graphene under a homogeneous magnetic field report non-integer conductance plateaus for gate-tunable bipolar junctions[3, 4]. The topological nature of the quantum Hall system has been clearly understood via the presence of robust edge states which are topologically protected[5, 6]. The bulk-boundary correspondence gives us an intuitive way of understanding the properties of these topological edge states: the number of conducting channels is characterized by the topological invariant of the quantum Hall insulator[7–9]. It has been well known that the topological invariant (or so-called Chern number) of a quantum Hall insulator is given by the filling factor in the integer quantum Hall effect[10–13].

The observation of non-integer conductance plateaus in bipolar graphene quantum Hall systems has been interpreted by the equilibration of topological states at the interface, and theoretical efforts have supported experimental findings by considering disorders on the edges and interface[14–17]. Despite the agreement between theoretical supports and experimental measurements for small filling factor cases, there are still open questions for relatively larger filling factorsnamely, the incompleteness of the equilibration and its origin. Recently, it has been theoretically revealed that the equilibration of the topological states at a Chern insulator junction can deteriorate if the junction is not perfectly fabricated, thereby limiting the interplay between higher-order Landau level (LL) states[17]. Junction conductance via interface equilibration has also been reported for p-n-p junctions in quantum Hall graphene systems[18, 19], with the consideration that there can be reflections at the bipolar junction. Despite efforts to understand the interplay behaviour of the topological interface states using multi-terminal conductance[18, 20], verification of the predicted reflections at the junction interfaces is still desired and can be obtained by delving into exactly how the states behave at a Chern insulator junction.

In this study, a four-terminal geometry is considered to allow the examination of the longitudinal and quantum Hall conductance via different leads, individually. As the states are topologically protected, they are robust against disorders which results in a lack of backscattering. Thus, it is straightforward to predict that the states are split into two directions

along the edges. Even in two-terminal conductance studies, the splitting of the topological interface states is also expected but is indirectly reflected in the resulting conductance plateaus across junctions. The four-terminal geometry considered in this work allows us to independently detect both left- and right-split modes from the topological interface states via two individual leads; additionally, the typical edge states are also measured via the longitudinal conductance (see Fig. 1). Here, the sum of the two split conductances must be equal to the typical quantum Hall conductance because of flux conservation. We also take into account random roughness effects and model a more realistic profile of the junction. Overall, the four-terminal conductance with flux conservation of the topological interface states provides an intuitive way of understanding how the interplay between the states occurs at the junction interface.

## RESULTS

### Theoretical approaches to topological interface states

In terms of topology, the bipolar junction of graphene in the quantum Hall regime can be regarded as a Chern insulator junction, which is feasible to fabricate by applying a homogeneous magnetic field to graphene where a bipolar junction is introduced via gated structures[3, 21](see Fig. 1). With an analytical approach, the effective Dirac Hamiltonian for graphene under a homogeneous magnetic field reads

$$H = \hbar v_F \vec{\sigma} \cdot \vec{\pi} + V(x), \quad (1)$$

where  $v_F = 10^6 \text{ ms}^{-1}$  is the Fermi velocity of graphene,  $\vec{\sigma} = (\sigma_1, \sigma_2)$  are the Pauli matrices,  $\vec{\pi} = \vec{p} + e\vec{A}$ , and the electrostatic potential is given by

$$V(x) = \frac{V_2 - V_1}{2} \tanh(x/\xi) + \frac{V_1 + V_2}{2}, \quad (2)$$

which becomes an abrupt potential step for  $\xi = 0$ . The Dirac equation with the above effective Hamiltonian,  $H\Psi = E\Psi$  with  $\Psi = (\psi_A, \psi_B)^T$ , consists of two sublattice-coupled equations and becomes analytically solvable by decoupling them, resulting in the following Schrödinger-like second-order differential equation:

$$\left\{ \frac{d^2}{dx^2} - \frac{\varsigma}{2} - \left( k_y + \frac{x}{2} \right)^2 + [E - V(x)]^2 \right\} \psi_{A,B} = 0, \quad (3)$$

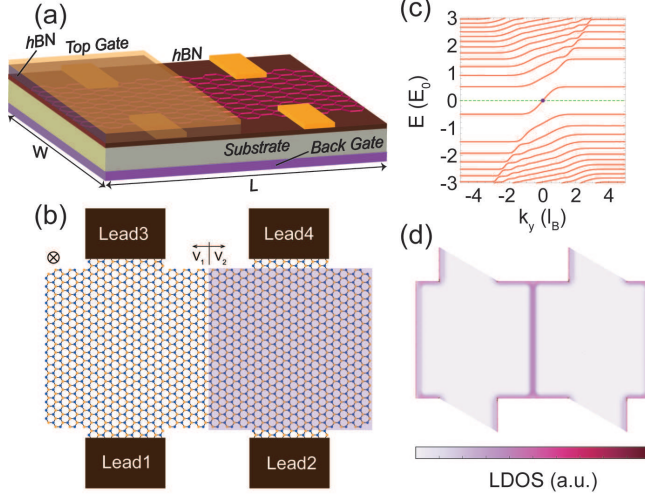


FIG. 1. (a) Schematic diagram of the gated structure considered in this study. (b) Depiction of the four-terminal graphene Hall bar with a bipolar junction exploiting the above gated structure. (c) Eigenenergies of the system with  $V_1 = -V_2 = -E_0/2$  at  $B = 30$  T. The dashed line represents the given Fermi energy  $E_F = 0$  and the dot marks the intersection of the Fermi energy and the eigenenergies, indicating the existence of interface states. (d) Local density of states of the same system as (c). The light and dark colours represent low and high densities, respectively.

where  $\varsigma = \pm 1$  for different sublattices, and  $k_y$  is the  $y$ -component momentum which acts as a good quantum number since  $[H, p_y] = 0$ . The above equation is dimensionless upon  $E_0 = \sqrt{2\hbar v_F^2 e B}$  and  $l_B = \sqrt{\hbar/(2eB)}$ , and we choose the Landau gauge, i.e.,  $\vec{A} = (0, Bx, 0)$ , which leads to  $\vec{B} = (0, 0, B)$ . Eq. (3) can be regarded as if Dirac fermions experience the effective potential given by  $V_{eff} = \varsigma/2 + (k_y + x/2)^2$ , and the solutions for  $\psi_A$  and  $\psi_B$  are obtained as parabolic cylinder functions in the low-energy limit[22–25]:

$$\Psi(x) = \begin{pmatrix} \psi_A(x) \\ \psi_B(x) \end{pmatrix} = A \begin{pmatrix} D_{n-1}(\zeta) \\ \frac{is}{\sqrt{n}} D_n(s\zeta) \end{pmatrix}, \quad (4)$$

where  $n \equiv (E - V_{1,2})^2$  for each region with the potential  $V_{1,2}$ ,  $\zeta \equiv 2k_y + x$ , and  $s = \text{sign}(x)$ . Note that the normalization factor is found to be  $A = [16\pi(n-1)!^2]^{1/4}$ .

Alternatively, the tight-binding approach also accounts for the present system, leading to the following Hamiltonian:

$$H = \epsilon_i \sum_i c_i^\dagger c_i + t_{ij} \sum_{\langle i,j \rangle} (c_i^\dagger c_j + h.c.) \quad (5)$$

where  $\epsilon_i$  is the on-site energy including the potential step (Eq. (2)), and  $c_i^\dagger$  and  $c_i$  are the creation and annihilation operators on the  $i$ -th site. In the presence of a magnetic field, the hopping term is defined by

$$t_{ij} = te^{i\frac{2\pi}{\Phi_0} \int_{r_i}^{r_j} \vec{A} \cdot d\vec{r}}, \quad (6)$$

where  $t = 3.0$  eV is the hopping energy, and  $\Phi_0 = e/h$  is the flux quantum. Here, we choose the same gauge considered in the analytical approach. Note that the system is centered at  $\vec{r} = (0, 0)$ . According to the defined potential profile, the system is divided into two regions where the lowest LLs are located at  $E = -V_1$  and  $-V_2$ . The ballistic conductance of the four-terminal graphene Hall bar is calculated in the linear response regime, exploiting the Landauer-Büttiker approach, as

$$G_{\alpha\beta}(E) = \frac{e^2}{h} \sum_{\alpha, \beta} |S_{\alpha\beta}(E)|^2, \quad (7)$$

where  $S_{\alpha\beta}$  is the scattering matrix from lead  $\beta$  to  $\alpha$ . With the tight-binding Hamiltonian, we can also take local density of states (LDOS) at a given energy:

$$\rho(\vec{r}_i, E) = \sum_m |\langle m | \Psi(\vec{r}_i) \rangle|^2 \delta(E - E_m), \quad (8)$$

where  $\Psi(\vec{r}_i)$  is the eigenfunction of the Dirac Hamiltonian, and  $|m\rangle$  specifies  $p_z$  orbital eigenstates of graphene with energy  $E_m$ . In addition, the probability density of the scattering region for the incoming wavefunction through a given lead is calculated by

$$P(\vec{r}_i, E) = |\Psi^\dagger(\vec{r}_i, E) \Psi(\vec{r}_i, E)|^2 \quad (9)$$

to provide useful information on how the current actually flows.

Both analytic and tight-binding approaches to understanding the electronic and transport properties of the system are in agreement with each other. In particular, formation of the interface states at the bipolar junction is demonstrated by the eigenenergy bands, which are obtained by using wavefunction continuity conditions at the interface,  $x = 0$  (see Fig. 1(c)). For given potentials  $V_1 = -V_2 = E_0/2$ , one can see that a conducting channel must exist between electron and hole-doped regions at  $E_F = 0$ , connecting the same-index LLs. For the same potential, the existence of the interface channels is also ensured by the LDOS at  $E_F = 0$  from the tight-binding approach using the KWANT code[26]. It is worth mentioning

that the occurrence of the metallic channels along the interface of the bipolar junction is due to the bulk-boundary correspondence; therefore, the interface states are topologically protected. The number of topological interface states is in keeping with the Chern number configuration of the bipolar junction in the quantum Hall graphene system. In fact, the Chern number of the quantum Hall insulator is derived from the TKNN formalism[5], and the Chern number of each region turns out to be the filling factor. Note that, here, we define the odd-number filling factor of the graphene quantum Hall regime in units of  $2e^2/h$ , distinct from the even-number filling factor in units of  $e^2/h$ . Since the topological interface states are doubly degenerate because of valley symmetry, the single channel at the interface in both Figs. 1c and d actually contains two topological states, and the number of the topological interface states equals the Chern number difference for  $(\mathcal{C}_1, \mathcal{C}_2) = (1, -1)$ .

#### **Four-terminal conductance and splitting nature in ballistic regime**

As reported in previous studies[3, 4], in bipolar quantum Hall graphene, the topological interface states exist only in case of p-n junctions on the basis of the equilibration concept. For a two-terminal geometry, conductance measurements through the bipolar junctions are attributed to either the mode-mixing between parallel-propagating states at the p-n junction interface or edge modes along the system boundary in case of n-n' (p-p') junctions, according to the polarity of the bipolar junctions. Since the system is finite, the conducting channel along the interface states ends up split into opposite directions, resulting in reflection modes that have been indirectly measured[18, 20]. On the other hand, using four-terminal geometry, here we are able to measure the splitting of the conductance through the topological interface states with two individual transverse conductances  $G_{31}$  and  $G_{41}$  which are taken between leads 1 and 3 or 4, as displayed in Fig. 1(b). In addition, we also take into account the longitudinal conductance  $G_{21}$  to detect the edge state contribution to the conductance in case of n-n' (p-p') junctions.

Figure 2(a) shows the calculated conductances for the given bipolar junction  $V_1 = -V_2 = E_0/2$  as functions of Fermi energy. In this case, the bipolar junction can be regarded as a Chern insulator junction where a topological interface is formed between  $\mathcal{C}_1 = +1$  and  $\mathcal{C}_2 = -1$  regions. When  $|E_F| < E_0/2$ , the topological states are formed at the junction interface, resulting in  $G_{31}$  and  $G_{41}$  along the interface which are split into the individual

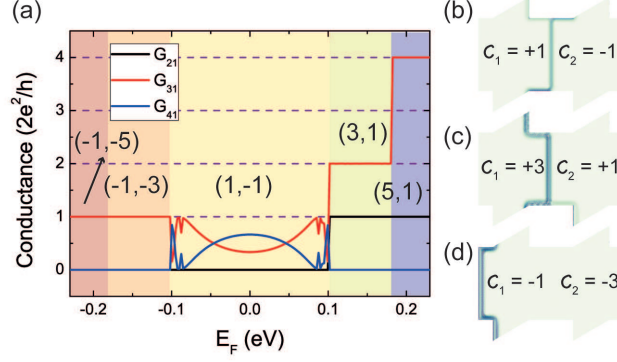


FIG. 2. (a) Four-terminal conductance of bipolar graphene in the quantum Hall regime. The coloured regions represent various Chern insulator junction cases with different Chern number configurations,  $(C_1, C_2)$ , depending on the Fermi energy. The dashed lines display quantized conductance values. (b), (c), and (d) Probability densities of the propagating modes, coming in from lead 1, at Fermi energies  $E_F = 0$ ,  $0.15$ , and  $-0.15$  eV, respectively. The four leads are identical to those depicted in Fig. 1(b). The applied magnetic field strength is approximately 30 T, being consistent with Fig. 1(c).

leads. One can clearly see that the sum of the two individual transverse conductances becomes  $2e^2/h$ , which is equal to the quantum Hall conductance plateau from the lowest-LL states[1]. Besides, it is seen that  $G_{21}$  vanishes for  $|E_F| < E_0/2$ , because the incoming mode wholly propagates along the interface, as shown in Fig. 2(b). For  $E_F < -E_0/2$ , the longitudinal conductance  $G_{21}$  from lead 1 to 2 is also expected to be zero due to the propagation of the edge states along the system boundary in the opposite direction, i.e., from lead 2 to 1. By the same token,  $G_{31}$  and  $G_{41}$  also vanish for  $E_F < -E_0/2$  with the reversal of the propagating direction of the edge states in the whole system, as displayed in Fig. 2(c). Interestingly, for  $E_F > E_0/2$ , while  $G_{31}$  exhibits typical quantum Hall conductance plateaus as  $E_F$  varies, the plateaus are smaller by a factor of  $e^2/h$  since one topological channel (correlated to the lowest LLs) is canceled out at the n-n' junction interfaces (see Fig. 2(d)). Further, for  $E_F > E_0/2$ ,  $G_{12}$  shows the same results as those reported from two-terminal conductance measurements[3]. However,  $G_{41}$  is found to be non-zero only for  $|E_F| < E_0/2$  because the transverse conductance across the junction can only be attributed to the existence of topological interface states and their interplay. Therefore, the existence of nonzero  $G_{41}$  is direct evidence that this interplay occurs at the Chern insulator junction.

Moreover, while there is no plateau for  $|E_F| < E_0/2$ , the conductance values vary depending on  $E_F$ . It has been shown that roughness on both edges and interfaces leads to ballistic-Ohmic transitions in the quantum Hall conductance plateaus, by demonstrating that experimental observations in the Ohmic limit are distinct from quantum Hall conductance in the ballistic limit[15]. Here, our approach to four-terminal conductance is in the ballistic limit, which necessitates the introduction of the roughness effects in order to treat the system more realistically. Edge roughness is randomly generated by  $W_{rough} = W + \delta W$  where

$$\delta W = \frac{3}{8} [\sin(\gamma_1 x) + \sin(\gamma_2 x)]. \quad (10)$$

Here,  $\gamma_1$  and  $\gamma_2$  are independent random numbers within range  $[0.1L : 0.15L]$ , and the root mean square roughness is about  $0.53 l_B$ .

### Edge roughness effects on interplay between topological interface states

Figure 3 shows the effects of edge roughness on the four-terminal conductance of bipolar graphene in the quantum Hall regime. For  $|E_F| < E_0/2$ , both  $G_{31}$  and  $G_{41}$  now exhibit clear plateaus. The plateaus appear at  $e^2/h$ , indicating an equal split into the two individual leads. The roughness-induced conductance plateau can be intuitively understood by the valley-isospin dependent quantum Hall conductance of armchair graphene nanoribbons[15, 27, 28]. We find that the resulting conductance plateau  $e^2/h$  in Fig. 3(a) is equal to the mean of the conductance values for three different armchair graphene nanoribbon cases:  $2\frac{e^2}{h}$  for the metallic case, and  $\frac{1}{2}\frac{e^2}{h}$  for the two semiconducting cases[29, 30]. In other words, quantum Hall conductance through a bipolar junction is expected to be three-fold, depending on the size of the armchair graphene nanoribbons. As previously mentioned, randomly distributed edge roughness allows the system to contain those three different ribbon widths. Additionally, the four-terminal conductance results satisfy flux conservation: the incoming flux from lead 1 is given by  $2e^2/h$  because there is a single metallic channel due to  $\mathcal{C}_1 = 1$ , and the sum of  $G_{31}$  and  $G_{41}$  is equal to  $2e^2/h$ , resulting in  $G_{21} = 0$ . The half-and-half conductance splitting leads to the conclusion that the interplay of the topological interface states from the lowest LLs undergoes full mixing.

Compared to the lowest-LL case, the interplay nature between higher-index LLs at the



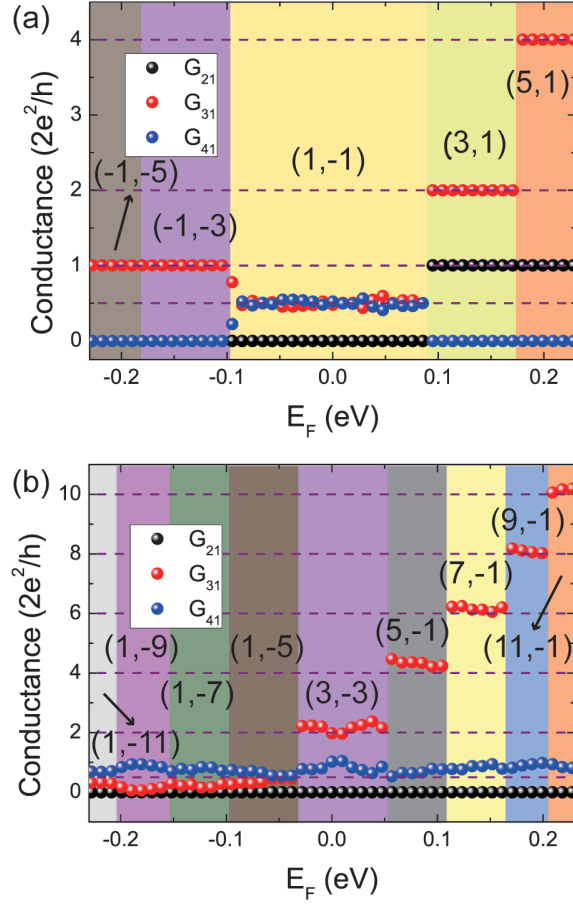


FIG. 3. Four-terminal conductances in the presence of edge roughness for the given junction; (a)  $V_1 = -V_2 = E_0/2$  and (b)  $V_1 = -V_2 = (1 + \sqrt{2}) E_0/2$  as functions of  $E_F$ . The dashed lines are guiding lines corresponding to the individual plateaus, and the shaded regions represent different Chern number configurations  $(\mathcal{C}_1, \mathcal{C}_2)$ . Results are obtained by averaging over 100 randomly distributed edge roughness sets.

bipolar junction in quantum Hall graphene is more complicated. Figure 3(b) shows the four-terminal conductance results in the presence of edge roughness for  $\mathcal{C}_1 = -\mathcal{C}_2 = 3$ , where two topological edge modes exist in each region. Note that the contribution of these topological states to the conductance is given by  $3 \times 2e^2/h$  because the higher-index LL is doubly degenerate compared to the lowest LL. Around  $E_F = 0$  it is seen that  $G_{31}$  is twice as large as  $G_{41}$ , satisfying flux conservation, i.e.,  $G_{31} + G_{41} = 3 \times 2e^2/h$ . This asymmetric splitting behaviour can be explained by considering the Chalker-Coddington type argument,

where it has been confirmed that the interplay of topological states at the interface can be expressed as a transfer matrix representation[15, 31, 32]. In the case of  $\mathcal{C}_1 = -\mathcal{C}_2 = 3$ , there are four modes in total with the corresponding transfer matrix reading[15]

$$\mathbf{M} = \begin{pmatrix} \Xi_1 & -\Sigma_1 & 0 & 0 \\ \Sigma_1 & \Xi_1 & 0 & 0 \\ 0 & 0 & \Xi_0 & \Sigma_0 \\ 0 & 0 & \Sigma_0 & \Xi_0 \end{pmatrix}, \quad (11)$$

where  $\Xi_{0,1} = \cos \theta_{0,1}$ ,  $\Sigma_{0,1} = \sin \theta_{0,1}$ . Here,  $\theta_{0,1}$  indicates the degree of interplay between the lowest- (1st-) LL topological interface states, and  $\theta = \pi/4$  gives rise to the half-and-half mixing between the states. For  $\theta = 0$ , there is no interplay, whereas for  $\theta = \pi/2$ , the incoming mode from one region completely transfers to the other region. Note that the matrix  $\mathbf{M}$ , which is composed of two diagonal block matrices, implies no coupling between the lowest- and 1st-LL topological states due to the orthogonality of the solutions (see Eq. (4)). In other words, the orthogonality allows for interplay between the time-reversal partners, based on the fact that particle-hole symmetry exists in the system. As previously stated, the lowest-LL topological states undergo half-and-half mixing, resulting in  $\theta_0 = \pi/4$ , while on the other hand,  $\theta_1$  is expected to be somewhere between 0 and  $\pi/2$ . With the given  $\theta_0 = \pi/4$ ,  $\theta_1$  can be found using the transfer matrix with the following equation:

$$\Psi_f = \mathbf{M}\Psi_i, \quad (12)$$

where  $\Psi_f = (|1; n\rangle, |1; p\rangle, |0; n\rangle, |0; p\rangle)^T$  and  $\Psi_i = (|1; n\rangle, 0, |0; n\rangle, 0)^T$ . Note that, for  $\Psi_f$ ,  $|1; n\rangle$  and  $|0; n\rangle$  are electron-type topological states corresponding to  $G_{31}$ , and  $|1; p\rangle$  and  $|0; p\rangle$  are hole-type states corresponding to  $G_{41}$ . For  $\mathcal{C}_3 = -\mathcal{C}_2 = 3$ ,  $\theta_1$  is found to be about  $\pi/6$ , resulting in  $G_{31} \approx 4e^2/h$  and  $G_{41} \approx 2e^2/h$  as shown in Fig. 3(b). Consequently, the higher-LL topological states are expected to be moderately equilibrated at the Chern insulator junction. Moreover, it is worth investigating the interplay behaviour for asymmetric Chern number configurations, e.g.,  $(5, -1)$  and  $(7, -1)$ , as displayed in Fig. 3(b). Unlike the symmetric cases, higher-LL topological states have no time-reversal partner for interplay, differing from the lowest-LL states. However, because of the asymmetry, the interplay between the lowest-LL states can be changed, making  $\theta_0 \neq \pi/4$  no longer true. Indeed, it is straightforward to find values of  $\theta_0$  for various asymmetric configurations of Chern numbers,

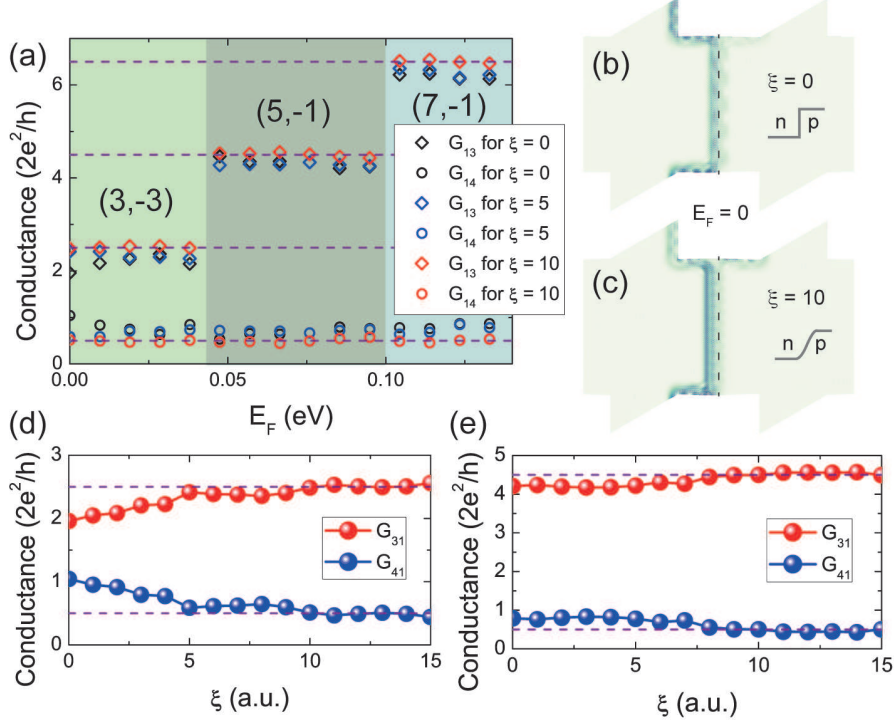


FIG. 4. (a) Split quantum Hall conductances  $G_{31}$  and  $G_{41}$  as functions of  $E_F$  for different potential profiles of the bipolar junction. The case of the abrupt potential step is characterized by the parameter  $\xi = 0$ . The diamonds and circles represent  $G_{31}$  and  $G_{41}$ , respectively. The dashed lines are guiding lines for the split conductance values in the suppression limit, with coloured regions indicating different Chern number configurations for the bipolar junction, the same as those in Fig. 3(b). (b) and (c) Colour maps of the probability densities at  $E_F$  for the abrupt ( $\xi = 0$ ) and gradual ( $\xi = 10$ ) junctions, respectively. The light and dark colours represent low and high densities, respectively. The four leads are labeled in the same manner as Fig. 1(b). Schematic diagrams of each junction are displayed as insets. (d) and (e)  $G_{31}$  and  $G_{41}$  versus  $\xi$  at  $E_F = 0.04$  and  $0.08$  corresponding to different Chern number configurations  $(1, -1)$  and  $(3, -3)$ , respectively. The dashed lines are guiding lines corresponding to the suppressed values of  $G_{31}$  and  $G_{41}$ .

based on the Chalker-Coddington type argument:  $\theta_0 = 3\pi/10$  for  $(5, -1)$ ,  $2\pi/5$  for  $(7, -1)$ , and so on.

## Suppression of topological interplay with gradual potential

As discussed above, the mixing nature of the topological interface states at the Chern insulator junction is fairly complicated because a number of interface states can be coupled to each other like as a network, and behave according to the Chalker-Coddington argument. On the other hand, there have been findings where mode-mixing at the Chern insulator junction can be limited to the lowest-LL mode in the presence of a depletion spacer[14, 15, 17]. In fact, realistic device fabrication inevitably causes a smoothening of the potential step for the bipolar junction, which can be described by Eq. (2). By varying the parameter  $\xi$  from the potential profiles (Eq. (2)), the gradualness of the smoothly varying potential profile can be tuned. As expected, sufficiently large values of  $\xi$  lead to a reduction in  $G_{41}$ , ending up with clear plateaus at  $e^2/h$  regardless of the Chern number configurations, as shown in Fig. 4(a). The reduced conductance from lead 1 to 4 implies that the interplay between topological states is limited to the lowest LLs as recently discussed[17]. In other words, suppression of the interplay occurs only for the higher-index LLs. An intuitive explanation for this suppression phenomena can be found by analyzing the probability density when the potential profiles become gradual. Figures 4(b) and (c) provide a comparison of the probability density of the scattering region between the abrupt and gradual potential profiles. It is clearly seen that the topological interface states are spatially impelled toward the interior of the system, so that the degree of the interplay at the interface decreases. It is speculated that the lowest-LL topological states are formed at  $x = 0$ , where the potential strength is exactly zero, so that the topological states at  $x = 0$  are almost unaffected by the gradual potential profile. Higher-index LL topological states though are further separated by the gradually varying potentials.

Regarding the mode-mixing suppression, it is natural to expect that the suppression of the interplay between the topological interface states depends on the gradualness of the junction profile. Indeed, Figs. 4(d) and (e) confirm that  $G_{41}$  for the  $(1, -1)$  case reaches  $e^2/h$  more rapidly than for the  $(3, -3)$  case, as  $\xi$  varies. As expected, the interplay ends up being attributed to the lowest-LL states only, for the sufficiently gradual potential profiles. Therefore, a careful analysis of the conductance plateaus is required to correctly understand the quantum Hall measurements through bipolar junctions, including an examination of potential profile steepness. Depending on the slope of the potential profile near the interface,

the degree of interplay between topological states can vary, likely resulting in unclear plateau values.

## **DISCUSSION**

In summary, we have exploited four-terminal quantum Hall conductance through a bipolar junction in graphene to understand the interplay nature of the topologically protected states at the junction interface. The properties of the topological interface states are examined not only by numerical calculations but also analytic solutions, which are in agreement with each other. We have studied the influence of edge roughness on the splitting of the quantum Hall conductance due to the interplay between the topological interface states. From the resulting quantum Hall conductance plateaus, we have deduced the degree of interplay for various Chern number configurations using the Chalker-Coddington type argument.

We conclude by remarking that, in general, the interplay between topological interface states is described by partial equilibration at a clean interface, as distinct from full equilibration at a rough interface. Moreover, for realistic bipolar junctions in graphene, interplay between higher-LL topological states tends to be suppressed as the potential profiles become gradual. Such a suppression of the interplay phenomena occurs because the higher-LL topological states become spatially farther away from the interface for gradually varying potentials. Our findings in this study provide a good predictive way of elucidating the interplay behaviour of quantum Hall graphene systems.

## **ACKNOWLEDGEMENT**

This work was sponsored by project code (IBS-R024-D1).

## **ADDITIONAL INFORMATION**

### **Author contributions**

NM set up the problem and the corresponding system for both analytical and numerical studies. NM carried out the calculations and analyse the calculated results upon discussion with HCP. NM and HCP wrote the manuscript.

## Competing interests

The authors declare no competing financial interest.

## Corresponding author

Correspond to H. C. Park.

---

\* hcpark@ibs.re.kr

- [1] K. S. Novoselov, A. K. Geim, S. V. Morozov, D. Jiang, M. I. Katsnelson, I. V. Grigorieva, S. V. Dubonos and A. A. Two-dimensional gas of massless Dirac fermions in graphene *Nature (London)* **438**, 197-200 (2005).
- [2] A. H. Castro Neto, F. Guinea, N. M. R. Peres, K. S. Novoselov and A. K. Geim The electronic properties of graphene *Rev. Mod. Phys.* **81**, 109 (2009).
- [3] J. R. Williams, L. DiCarlo and C. M. Marcus Quantum Hall effect in a gate-controlled  $p$ - $n$  junction of graphene *Science* **317**, 638-641 (2007).
- [4] D. A. Abanin and L. S. Levitov Quantized transport in graphene  $p$ - $n$  junctions in a magnetic field *Science* **317**, 641-643 (2007).
- [5] Y. Hatsugai Chern number and edge states in the integer quantum Hall effect *Phys. Rev. Lett.* **71**, 3697 (1993).
- [6] C. L. Kane and E. J. Mele  $Z_2$  topological order and the quantum spin Hall effect *Phys. Rev. Lett.* **95**, 146802 (2005).
- [7] B. I. Halperin Quantized Hall conductance, current-carrying edge states, and the existence of extended states in a two-dimensional disordered potential *Phys. Rev. B* **25**, 2185 (1982).
- [8] A. M. Essin and V. Gurarie Bulk-boundary correspondence of topological insulators from their respective Green's functions *Phys. Rev. B* **84**, 125132 (2011).
- [9] S. Matsuura, P.-Y. Chang, A. P. Schnyder and S. Ryu Protected boundary states in gapless topological phases *New J. Phys.* **15** 065001 (2013).
- [10] D. J. Thouless, M. Kohmoto, M. P. Nightingale and M. den Nijs Quantized Hall conductance in a two-dimensional periodic potential *Phys. Rev. Lett.* **49** 405 (1982).

- [11] F. D. M. Haldane Model for a quantum Hall effect without Landau levels: Condensed-matter realization of the “Parity Anomaly” *Phys. Rev. Lett.* **61**, 2015 (1988).
- [12] M. Z. Hasan and C. L. Kane Colloquium: Topological insulators *Rev. Mod. Phys.* **82**, 3045 (2011).
- [13] Y. Ando Topological insulator materials *J. Phys. Soc. Jpn.* **82**, 102001 (2013).
- [14] J. Li and S.-Q. Shen Disorder effects in the quantum Hall effect of graphene  $p$ - $n$  junctions, *Phys. Rev. B* **78**, 205308 (2008).
- [15] T. Low Ballistic-Ohmic quantum Hall plateau transition in a graphene  $p$ - $n$  junction *Phys. Rev. B* **80**, 205423 (2009).
- [16] C. Fräßdorf, L. Trifunovic, N. Bogdanoff and P. W. Brouwer Graphene  $pn$  junction in a quantizing magnetic field: Conductance at intermediate disorder strength *Phys. Rev. B* **94**, 195439 (2016).
- [17] S. W. LaGasse and J. U. Lee Theory of Landau level mixing in heavily graded graphene  $p$ - $n$  junctions *Phys. Rev. B* **94**, 165312 (2016).
- [18] D.-K. Ki and H.-J. Lee Quantum Hall resistances of a multiterminal top-gated graphene device *Phys. Rev. B* **79**, 195327 (2009).
- [19] S. Debey and M. M. Deshmukh Tuning equilibration of quantum Hall edge states in graphene - Role of crossed electric and magnetic fields *Solid State Commun.* **237-238**, 59-63 (2016).
- [20] D.-K. Ki, S.-G. Nam, H.-J. Lee and B. Özyilmaz Dependence of quantum-Hall conductance on the edge-state equilibration position in a bipolar graphene sheet *Phys. Rev. B* **81**, 033301 (2010).
- [21] B. Özyilmaz, P. Jarillo-Herrero, D. Efetov, D. A. Abanin, L. S. Levitov and P. Kim Electronic transport and quantum Hall effect in bipolar graphene  $p$ - $n$ - $p$  junctions *Phys. Rev. Lett.* **99**, 166804 (2007).
- [22] L. Oroszány, P. Rakya, A. Kormányos, C. J. Lambert and J. Cserti Theory of snake states in graphene *Phys. Rev. B* **77**, 081403(R) (2008).
- [23] S. Park and H.-S. Sim Magnetic edge states in graphene in nonuniform magnetic fields *Phys. Rev. B* **77**, 075433 (2008).
- [24] T. K. Ghosh, A. De Martino, W. Hässler, L. Dell’Anna and R. Egger Conductance quantization and snake states in graphene magnetic waveguides *Phys. Rev. B* **77**, 081404(R) (2008).

- [25] L. Cohnitz, A. De Martino, W. Hässler and R. Egger Chiral interface states in graphene  $p$ - $n$  junctions *Phys. Rev. B* **94**, 165433 (2016).
- [26] C. W. Groth, M. Wimmer, A. R. Akhmerov and X. Waintal Kwant: a software package for quantum transport *New J. Phys.* **16**, 063065 (2014).
- [27] J. Tworzydło, I. Snynam, A. R. Akhmerov and C. W. Beenakker Valley-isospin dependence of the quantum Hall effect in a graphene  $p$ - $n$  junction *Phys. Rev. B* **76**, 035411 (2007).
- [28] A. Mreńca-Kolasińska, S. Heun and B. Szafran Aharonov-Bohm interferometer based on  $n$ - $p$  junctions in graphene nanoribbons *Phys. Rev. B* **93**, 125411 (2016).
- [29] K. Nakada, M. Fujita, G. Dresselhaus and M. S. Dresselhaus Edge state in graphene ribbons: Nanometer size effect and edge shape dependence *Phys. Rev. B* **54**, 17954 (1996).
- [30] Y.-W. Son, M. L. Cohen and S. G. Louie Energy gaps in graphene nanoribbons *Phys. Rev. Lett.* **97**, 216803 (2006).
- [31] J. T. Chalker and P. D. Coddington Percolation, quantum tunneling and the integer Hall effect *J. Phys.: Condens. Mater.* **21**, 2665-2679 (1988).
- [32] D.-H. Lee, Z. Wang and S. Kivelson Quantum percolation and plateau transitions in the quantum Hall effect *Phys. Rev. Lett.* **70**, 4130 (1993).